

Coupled Analyses of Excavations in Saturated Soil

Christianne de Lyra Nogueira, D.Sc.¹; Roberto Francisco de Azevedo, Ph.D.²; and Jorge Gabriel Zornberg, Ph.D., P.E., M.ASCE³

Abstract: This paper presents finite-element analyses of excavations by using a coupled deformation and flow formulation. Specific numerical procedures were implemented into the finite-element codes to simulate the excavation construction and to solve the nonlinear coupled system. The paper discusses results of two generic excavations, with analyses conducted using different constitutive models and different excavation rates. Although the constitutive model affected the magnitude and distribution of the excess of the pore-water pressure due to the excavation process, the constitutive models only slightly influenced the dissipation rate of the excess pore-water pressure. Excavation rates that were one order of magnitude smaller than the hydraulic conductivity of the soil led to results representative of drained processes. Because of the slow rate needed for drained conditions, partially drained conditions normally prevail during excavations, highlighting the importance of coupled analyses.

DOI: 10.1061/(ASCE)1532-3641(2009)9:2(73)

CE Database subject headings: Coupling; Excavation; Saturated soils; Finite element method; Deformation.

Introduction

In highly populated regions, the efficient use of underground space becomes critical, conducting frequent construction of excavations near existing structures. To avert damage of these structures, it becomes necessary to evaluate the movements caused by such construction.

To predict movements caused by excavations, the geotechnical engineer must consider factors such as the stress history, the stress-strain-strength characteristics of the soils, the rate of the excavation, and the construction sequence. In addition, the groundwater in many situations influences the behavior of excavations, boosting the need for models that consider the response of the soil skeleton and the pore water by coupling force-displacement analysis with excess pore-water pressure dissipation (i.e., coupled deformation and flow analyses).

Since the 1970s, many authors have investigated consolidation problems by considering a linear elastic constitutive behavior and plane strain condition (Christian and Bohemer 1970; Hwang et al. 1971, 1972; Yokoo et al. 1971; Ghaboussi and Wilson 1973; Booker and Small 1975; Sandhu et al. 1977). They presented different formulations based on the variational principle, the virtual work principle, and Galerkin's methods that provided a set of

first-order ordinary differential equations related to time. These approaches generally performed the time integration numerically, dividing the time into time steps. Among the simple step methods to solve these sets of differential equations, the most frequently used was the generalized trapezoidal family method in which the recurrence formula depends on the state variable rather than on its rate.

In the 1980s and early 1990s, initial studies were reported on coupled analyses using elastoplastic constitutive models (Carter et al. 1979; Richter 1979; Siriwardane and Desai 1981; Borja 1989, 1991). In this case, a set of nonlinear partial differential equations represents the coupled elastoplastic problem, generally solved by an incremental-iterative procedure in which, starting from an initial equilibrium configuration (where the pore-water pressure, displacement field, and strain and stress states are known), a new equilibrium configuration can be obtained in terms of displacements and pore-water pressure.

In theory, at each increment and for a selected tolerance, the iterative scheme satisfies the global equilibrium equations, the compatibility and boundary conditions, and the constitutive equations. However, the constitutive equation integration is not trivial because, even if the incremental strain magnitude on each iterative cycle is known, the way it varies across the incremental path is unknown. Therefore, it is necessary to use an accurate stress integration algorithm.

Marques (1984) used a simple stress integration algorithm to integrate the von Mises elastoplastic model, with linear strain hardening. Ortiz and Popov (1985), Sloan (1987), and Potts and Ganendra (1994) reported studies on stress integration algorithms where they discuss their importance, advantages, and disadvantages. The study presented in this paper shows a successful application of an explicit stress integration algorithm using subincrements with a size that varies proportionally to the strain increment (Zornberg 1989).

Another important aspect addressed in this study is the adequacy of the FEM to simulate excavation process. This issue is relevant because, due to the nature of FEM displacement formulations, on the elements interfaces only force equilibrium is satisfied. As stress equilibrium is not verified, early methods that

¹Associate Professor, Dept. of Mines Engineering, Federal Univ. of Ouro Preto, Campus Universitário, Ouro Preto, MG 35400-000, Brazil. E-mail: chris@em.ufop.br

²Titular Professor, Dept. of Civil Engineering, Federal Univ. of Viçosa, Campus Universitário, Viçosa, MG 36570-000, Brazil. E-mail: razevedo@ufv.br

³Fluor Centennial Associate Professor, Dept. of Civil Engineering, Univ. of Texas at Austin, 1 University Station C1792, Austin, TX 78712-0280. E-mail: zornberg@mail.utexas.edu

Note. Discussion open until September 1, 2009. Separate discussions must be submitted for individual papers. The manuscript for this paper was submitted for review and possible publication on May 9, 2008; approved on October 15, 2008. This paper is part of the *International Journal of Geomechanics*, Vol. 9, No. 2, April 1, 2009. ©ASCE, ISSN 1532-3641/2009/2-73-81/\$25.00.

used stress interpolation procedures to obtain the external force (Christian and Wong 1973; Chandrasekaram and King 1974) are improper to simulate excavations.

Mana (1978) presented a new procedure to calculate the external force based on the static equilibrium equation. However, Azevedo (1983) showed that this procedure is mesh dependent, i.e., the exact magnitude of the external force depends on the element size just below the excavation contour. To get accurate responses, rather small elements are necessary along the excavation contour. Nevertheless, many authors have used Mana's procedure in their analyses (Osaimi 1977; Azevedo 1983; Azevedo and Consoli 1988; Zornberg 1989; Azevedo et al. 2001).

Brown and Booker (1985), based on the work of Ghaboussi and Pecknold (1984), analyzed excavations using elastoplastic models and showed that Mana's procedure does not guarantee total equilibrium and propagates errors through the subsequent excavation stages. They proposed a new external force evaluation method that numerically integrates the stress, body, and superficial forces and obeys static equilibrium. Borja et al. (1989), using an elastic perfectly plastic constitutive model, showed that Brown and Booker's procedure provides a unique solution for any number of excavation stages. The analyses performed in this paper use Brown and Booker's procedure to simulate the excavation process and confirms that this procedure is mesh independent.

Some applications of the FEM simulate excavations using Brown and Booker's method, consolidation, and elastoplasticity. For example, Yong et al. (1989) used the FEM to simulate an unsupported excavation in Singapore, adopting a simple elastoplastic model. Holt and Griffiths (1992) used the FEM to assess the transient stability of an unbraced excavation in soil using a nonassociated elastoplastic model. They showed the influence of the excavation rate on the excavation stability. Afterwards, Griffiths and Li (1993) presented a theoretical study about transient stability of excavated soil slopes using the FEM and a nonassociative elastoplastic model based on Mohr-Coulomb criteria. They showed the influence of K_0 on the long- and short-term stability of the slopes. At about the same time, Whittle et al. (1993) presented a coupled flow deformation analysis of a deep braced excavation in Boston using the MIT-E3 elastoplastic constitutive model. Finally, Nogueira (1998) analyzed supported and unsupported excavations using elastic, nonlinear elastic, and elastoplastic constitutive models.

This paper provides additional insight into the analysis of excavations using the FEM by coupling deformation and flow process. Besides presenting the finite-element formulation equations, the paper shows the nonlinear approaches used to solve the problem at the global and local levels. Finite-element algorithms to simulate excavation constructions are discussed and new equations to calculate equivalent nodal forces for coupled and/or submersed excavations are presented. Finally, the paper illustrates the influence of the soil hydraulic properties, the rate of construction and of the selected constitutive model on the excavation performance.

Finite-Element Formulation of the Coupled Problem

Assuming that pore fluid and solid grains are incompressible, equations of equilibrium and continuity of a deformable, saturated porous medium in domain V with contour S can be obtained using Darcy's law and the effective stress principle, as follows:

$$\nabla_u^T[\boldsymbol{\sigma}' + p\mathbf{m}] - \mathbf{b} = \mathbf{0} \text{ in } V \quad (1a)$$

$$-\nabla_p^T\left(\mathbf{k}\left[\mathbf{a} + \frac{1}{\gamma_w}\nabla_p p\right]\right) + \mathbf{m}^T\nabla_u\dot{\mathbf{u}} = 0 \text{ in } V \quad (1b)$$

in which $\boldsymbol{\sigma}'$ =vector of effective stress; p =pore-water pressure; \mathbf{b} =body force vector; \mathbf{k} =hydraulic conductivity matrix; \mathbf{u} =displacement vector; and $\dot{\mathbf{u}}$ =displacement vector rate. ∇_u and ∇_p =differential operators for a plane condition of $\mathbf{m}^T=[1 \ 1 \ 1 \ 0]$, $\mathbf{a}^T=[0 \ 1]$.

Eq. (1) must attend the following boundary conditions:

$$\boldsymbol{\sigma}'\mathbf{n} = -\mathbf{T} \text{ on } S_\sigma \quad (2a)$$

$$\mathbf{u} = \mathbf{0} \text{ on } S_u \quad (2b)$$

$$\mathbf{v}\mathbf{n} = 0 \text{ on } S_v \quad (2c)$$

$$p = \bar{p} \text{ on } S_p \quad (2d)$$

in which \mathbf{v} =superficial flow vector. S_σ , S_u , S_v , and S_p are, respectively, parts of the domain contour S with prescribed force, displacement, flow, and pore-water pressure. Eq. (1) must also attend the following initial condition:

$$\nabla_p^T\mathbf{u} = 0 \text{ on } t = 0^+ \quad (2e)$$

in which t =real time.

Biot (1941) developed these equations for a linear elastic porous media. Other authors have developed extensions of these equations for physical and geometric nonlinearities (e.g., Carter et al. 1979; Borja 1986, 1989).

The following integral form of Eq. (1) can be obtained, using the virtual work principle:

$$\int_V \mathbf{u}^{*T}[\nabla_u^T(\boldsymbol{\sigma}' + p\mathbf{m}) - \mathbf{b}]dV = \mathbf{0} \quad (3a)$$

$$\int_V p^{*T}[-\nabla_p^T(\mathbf{k}(\mathbf{a} + (1/\gamma_w)\nabla_p p)) + \mathbf{m}^T\nabla_u\dot{\mathbf{u}}]dV = 0 \quad (3b)$$

in which \mathbf{u}^* and p^* =virtual displacement vector and pore-water pressure, respectively.

Applying the divergence theorem, integrating by parts, and using the boundary conditions presented in Eq. (2a)–(2e), Eq. (3) becomes:

$$-\int_V (\nabla_u\mathbf{u}^*)^T\boldsymbol{\sigma}'dV - \int_V (\nabla_u\mathbf{u}^*)^T p\mathbf{m}dV - \int_S \mathbf{u}^{*T}\mathbf{T}dS - \int_V \mathbf{u}^{*T}\mathbf{b}dV = \mathbf{0} \quad (4a)$$

$$\int_V (\nabla_p p^*)^T \mathbf{k} \mathbf{a} dV + \int_V (\nabla_p p^*)^T (1/\gamma_w) \mathbf{k} \nabla_p p dV + \int_V p^* \mathbf{m}^T \nabla_u \dot{\mathbf{u}} dV = 0 \quad (4b)$$

The finite-element formulation uses the following interpolation scheme:

$$\mathbf{u}^* = \mathbf{N}_u \hat{\mathbf{u}} \quad (5a)$$

$$p^* = \mathbf{N}_p \hat{p} \quad (5b)$$

in which $\hat{\mathbf{u}}$ and \hat{p} =vectors of nodal displacement and pore-water pressure, respectively. \mathbf{N}_u and \mathbf{N}_p =interpolation function matrices that depend on the type of adopted element (Nogueira 1998).

As $\hat{\mathbf{u}}$ and $\hat{\mathbf{p}}$ cannot be zero, the following equilibrium and continuity equations are obtained by substituting Eq. (5) into Eq. (4):

$$-\int_V \mathbf{B}_u^T \boldsymbol{\sigma}' dV - \mathbf{C}\hat{\mathbf{p}} = \mathbf{F}_T + \mathbf{F}_B \quad (6a)$$

$$-\mathbf{C}^T \hat{\mathbf{u}} - \mathbf{H}\hat{\mathbf{p}} = \mathbf{Q} \quad (6b)$$

in which $\mathbf{C} = \int_V \mathbf{B}_u^T \mathbf{m} \mathbf{N}_p dV$ = coupling matrix; $\mathbf{F}_T = \int_{S_\sigma} \mathbf{N}_u^T \mathbf{T} dS$ = nodal force vector equivalent to superficial forces \mathbf{T} ; $\mathbf{F}_B = \int_V \mathbf{N}_u^T \mathbf{b} dV$ = nodal force vector equivalent to body forces \mathbf{b} ; $\mathbf{H} = \int_V \mathbf{B}_p^T (1/\gamma_w) \mathbf{k} \mathbf{B}_p dV$ = flux matrix; $\mathbf{Q} = \int_V \mathbf{B}_p^T \mathbf{k} \mathbf{a} dV$ = nodal flow vector equivalent to body forces acting in the \mathbf{a} vector direction; $\mathbf{B}_u = \nabla_u \mathbf{N}_u$, and $\mathbf{B}_p = \nabla_p \mathbf{N}_p$.

Dividing the time domain in finite intervals Δt and considering a linear variation of the state variables, the incremental form of Eq. (6) is

$$\Delta \mathbf{N}^s + \Delta \mathbf{N}^w = \Delta \mathbf{R}_u \quad (7a)$$

$$-\mathbf{C}^T \Delta \hat{\mathbf{u}} - \alpha \Delta t \mathbf{H} \Delta \hat{\mathbf{p}} = \Delta \mathbf{R}_p \quad (7b)$$

in which $\Delta \mathbf{N}^s = -\int_V \mathbf{B}_u^T \Delta \boldsymbol{\sigma}' dV$ represents the increment of internal forces due to the increment of effective stress $\Delta \boldsymbol{\sigma}'$; $\Delta \mathbf{N}^w = -\mathbf{C} \Delta \hat{\mathbf{p}}$ represents the increment of internal forces due to the increment of pore-water pressure $\Delta \hat{\mathbf{p}}$; $\Delta \mathbf{R}_u = \Delta \mathbf{F} = \Delta \mathbf{F}_T + \Delta \mathbf{F}_B$ represents the increment of external forces applied in the current step; and $\Delta \mathbf{R}_p = \Delta t [\alpha \Delta \mathbf{Q} + (\mathbf{Q}_n + \mathbf{H} \hat{\mathbf{p}}_n)]$ represents the volume change in the current step.

The terms $\mathbf{C}^T \Delta \hat{\mathbf{u}}$ and $\alpha \Delta t \mathbf{H} \Delta \hat{\mathbf{p}}$ represent the volumetric changes due to the increment of the effective stress and the pore-water pressure occurred on time interval Δt . In addition, α is the time integration constant.

Eq. (7) can be written in the following compact form:

$$\boldsymbol{\psi}(\Delta \mathbf{d}) = \mathbf{F}_{\text{int}}(\Delta \mathbf{d}) - \mathbf{F}_{\text{ext}} \quad (8)$$

in which

$$\Delta \mathbf{d} = \begin{Bmatrix} \Delta \hat{\mathbf{u}} \\ \Delta \hat{\mathbf{p}} \end{Bmatrix} \quad (9)$$

$$\mathbf{F}_{\text{int}}(\Delta \mathbf{d}) = \begin{Bmatrix} \Delta \mathbf{N}^s + \Delta \mathbf{N}^w \\ -\mathbf{C}^T \Delta \hat{\mathbf{u}} - \alpha \Delta t \mathbf{H} \Delta \hat{\mathbf{p}} \end{Bmatrix} \quad (10)$$

$$\mathbf{F}_{\text{ext}} = \begin{Bmatrix} \Delta \mathbf{R}_u \\ \Delta \mathbf{R}_p \end{Bmatrix} \quad (11)$$

Nonlinear Solution Approaches

Solution at the Global Level

In the time marching process, updating \mathbf{d} should lead to the solution of the system at the end of each step:

$$\hat{\mathbf{d}}_{n+1} = \hat{\mathbf{d}}_n + \Delta \hat{\mathbf{d}} \quad (12)$$

in which $\Delta \hat{\mathbf{d}}$ = solution of Eq. (8) obtained by an iterative scheme. Nonlinearity is related to $\Delta \mathbf{N}^s$ parcel of the internal force [Eq. (10)]. The iterative process can be expressed as follows:

$$\hat{\mathbf{d}} = \Delta \hat{\mathbf{d}}^0 + \sum_{k=1}^{\text{iter}} \delta \Delta \hat{\mathbf{u}}^k \quad (13)$$

in which $\Delta \hat{\mathbf{d}}^0$ = predict solution; $\delta \Delta \hat{\mathbf{u}}^k$ = iterative correction; and iter = number of iterations necessary to achieve convergence in the current time step, from t_n to t_{n+1} .

The recurrence scheme of the Newton–Raphson method was implemented, with the iterative correction obtained as follows:

$$\delta \Delta \mathbf{d}^k = \mathbf{J}^{k-1} \{ \mathbf{F}_{\text{ext}} - \mathbf{F}_{\text{int}}^k \} \quad (14)$$

in which

$$\mathbf{J}^k = \left[\frac{\partial \mathbf{F}_{\text{int}}(\Delta \mathbf{d}^k)}{\partial \Delta \mathbf{d}} \right] = \begin{bmatrix} \mathbf{K}_t^k & -\mathbf{C} \\ -\mathbf{C}^T & -\alpha \Delta t \mathbf{H} \end{bmatrix} \quad (15)$$

is the Jacobian matrix of the k iteration. In this definition:

$$\mathbf{K}_t^k = \left\{ \frac{\partial \Delta \mathbf{N}^s}{\partial \Delta \hat{\mathbf{u}}} \right\}^k = \int_V \mathbf{B}_u^T \left\{ \frac{\partial \Delta \boldsymbol{\sigma}'}{\partial \Delta \boldsymbol{\varepsilon}} \right\} \mathbf{B}_u dV = \int_V \mathbf{B}_u^T \mathbf{D}_t^k \mathbf{B}_u dV \quad (16)$$

is the tangent stiffness matrix and \mathbf{D}_t^k = constitutive matrix that depends on the constitutive model.

The predict solution is obtained considering a linear variation of the stress through the strain path. In this case

$$\Delta \mathbf{d}^0 = \mathbf{J}^n \mathbf{F}_{\text{ext}} = \begin{bmatrix} \mathbf{K}^n & -\mathbf{C} \\ -\mathbf{C}^T & -\alpha \Delta t_n \mathbf{H} \end{bmatrix} \begin{Bmatrix} \Delta \mathbf{F}_n \\ \Delta t_n [\alpha \Delta \mathbf{Q} + (\mathbf{Q}_n + \mathbf{H} \hat{\mathbf{p}}_n)] \end{Bmatrix} \quad (17)$$

in which \mathbf{K}^n = stiffness matrix at the beginning of the current time increment, and

$$\Delta t_n = \Delta \lambda_t^0 t_a \quad (18a)$$

$$\Delta \mathbf{F}_n = \Delta \lambda_c^0 \mathbf{F} \quad (18b)$$

in which t_a = time necessary to execute a certain stage of the constructive process; \mathbf{F} = load applied in this stage; and $\Delta \lambda_c^0$ and $\Delta \lambda_t^0$ = the initial factors of load and time increment, respectively, given as input data. The ratio between $\Delta \lambda_c^0$ and $\Delta \lambda_t^0$ defines the rate of the constructive process.

In theory, for a certain tolerance, these incremental-iterative procedures ensure global equilibrium at each increment. However, proper selection of the size of the time and load increments is important, as small increments may increase the solution time and large increments may lead to difficult convergence in the iterative process. Therefore, for a generic load–time increment i , the following automatic determination of the factors of load and time increments, according to Crisfield (1981), were adopted:

$$\Delta \lambda_t^i = \Delta \lambda_t^{i-1} \sqrt{I_d / I_{i-1}} \quad (19a)$$

$$\Delta \lambda_c^i = \Delta \lambda_c^{i-1} \sqrt{I_d / I_{i-1}} \quad (19b)$$

in which I_d = number of desired iterations (given as input data) and I_{i-1} = number of iterations used in the previous increment until reaching convergence.

Solution at the Local Level

In order to evaluate the $\Delta \mathbf{N}^s$ parcel of Eq. (10) in each iterative cycle, it is necessary to integrate the constitutive equations at each Gauss point of the elements. The integration procedure should be carefully selected because, although it is possible to know the size of the strain increment at each iterative cycle [that should be

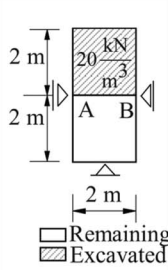
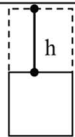
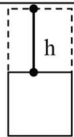
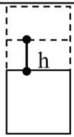
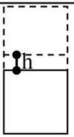
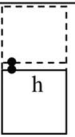
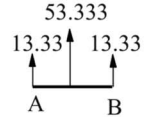
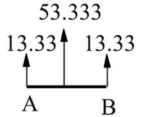
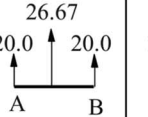
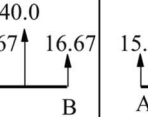
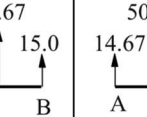
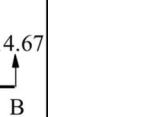
	Brown and Booker (1985)		Mana (1978)		
	 h=2m	 h=2m	 h=1m	 h=0.5m	 h=0.25m
 53.333 13.33 ↑ 13.33 A B	 53.333 13.33 ↑ 13.33 A B	 26.67 20.0 ↑ 20.0 A B	 40.0 16.67 ↑ 16.67 A B	 46.67 15.0 ↑ 15.0 A B	 50.0 14.67 ↑ 14.67 A B

Fig. 1. Equivalent nodal force provided by different excavation procedures

evaluated using the updated displacement increment, Eq. (13)], the corresponding stress increment is unknown for nonlinear materials.

Implicit or explicit stress integration algorithms are used to perform this integration. Although some authors claim that implicit algorithms are more precise, explicit algorithms are simpler. However, if the selection of subincrements is proper, explicit integration schemes can be as precise as implicit ones (Nayak and Zienkiewicz 1972; Sloan 1987; Sloan et al. 2001). Moreover, Potts and Ganenbra (1994) concluded that explicit integration schemes follow more closely actual strain paths. Consequently, this study uses an explicit algorithm as follows:

$$\Delta \boldsymbol{\sigma}' = \int_n^{n+1} \mathbf{D}_t d\boldsymbol{\varepsilon} \quad (20)$$

in which \mathbf{D}_t =constitutive tangent matrix. For elastoplastic materials, the constitutive tangent matrix is the elastoplastic constitutive matrix defined as

$$\mathbf{D}_t = \mathbf{D}_{ep} = \mathbf{D}_e - \left[\mathbf{D}_e \left[\frac{\mathbf{b}\mathbf{a}^T}{\mathbf{a}^T \mathbf{D}_e \mathbf{b} + H} \right] \mathbf{D}_e \right] \quad (21)$$

in which \mathbf{D}_e =elastic constitutive matrix; \mathbf{b} =gradient vector of the plastic strain increment; \mathbf{a} =gradient vector of the yield function $F(\boldsymbol{\sigma}', h)=0$; and H =hardening modulus defined as

$$H = - \frac{dF(\boldsymbol{\sigma}', h)}{dh} \left\{ \frac{dh}{d\varepsilon_p} \right\}^T \mathbf{b}(\boldsymbol{\sigma}', h) \quad (22)$$

in which h =hardening parameter. The infinitesimal increment of plastic strain is defined as

$$d\varepsilon_p = d\lambda \mathbf{b}(\boldsymbol{\sigma}', h) \quad (23)$$

in which the plastic parameter is given by

$$d\lambda = \frac{\mathbf{a}^T \mathbf{D}_e}{\mathbf{a}^T \mathbf{D}_e \mathbf{b} + H} d\boldsymbol{\varepsilon} \quad (24)$$

Eq. (24) holds for infinitesimal strains $d\boldsymbol{\varepsilon}$. As in any numerical procedure, the use of finite strain increments $\Delta \boldsymbol{\varepsilon}$ introduces an error in the calculation of $d\lambda$ [Eq. (24)]. Consequently, the consistency condition is not satisfied, forcing the use of special procedures. In order to minimize this error, Nayak and Zienkiewicz

(1972) proposed to divide the strain increment $\Delta \boldsymbol{\varepsilon}$ between increments n and $n+1$, in sub subincrements, as follows:

$$\Delta \boldsymbol{\sigma}' = \int_n^{n+1} \mathbf{D}_{ep} d\boldsymbol{\varepsilon} \approx \sum_{i=1}^{nsub} \mathbf{D}_{ep} (\Delta \boldsymbol{\varepsilon} / nsub) \quad (25)$$

Although many criteria determine the number of subincrements ($nsub$) (Nayak and Zienkiewicz 1972; Sloan 1987; Sloan et al. 2001), Zornberg (1989) suggested the following criterion:

$$nsub = \text{int} \left[\frac{\|\Delta \boldsymbol{\varepsilon}\|}{\varepsilon_{ref}} \right] + 1 \quad (26)$$

in which the reference strain ε_{ref} =thousandth fraction of the strain at soil failure obtained from a conventional compression triaxial test. The examples presented in this paper use this criterion.

Simulation of the Excavation Procedure

Fig. 1 shows results of a one-dimensional excavation of the top half of a soil column in terms of the nodal forces on the excavation contour AB . The equivalent nodal forces were obtained numerically by using Brown and Booker (1985) and Mana's (1978) procedures. Mana's procedure was conducted using different finite-element mesh in order to vary the element height h above of the contour AB .

Results show that Mana's procedure is highly dependent on the height of the finite element located right above the excavation boundary. This is because Mana's procedure uses the stress states in Gauss points of the excavated element to evaluate the nodal forces and these nodal forces are more accurately calculated when the Gauss points are closer to the excavation contour. On the other hand, Brown and Booker's procedure is mesh independent and thus more precise and convenient.

Brown and Booker (1985) determine the equivalent nodal forces as follows:

$$\mathbf{F}_i = \int_{V_i} \mathbf{B}^T \boldsymbol{\sigma}_{i-1} dV - \int_{V_i} \mathbf{N}^T \mathbf{b} dV - \int_{S_i} \mathbf{N}^T t dS \quad (27)$$

in which V_i =volume of all elements that remains in the finite-element mesh after excavation stage i , and S_i =corresponding contour.

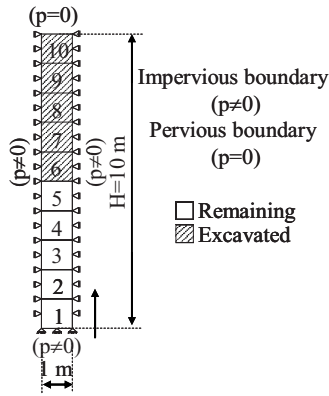


Fig. 2. One-dimensional excavation: finite-element mesh

The first term on the right-hand side of Eq. (27) represents nodal forces equivalent to total stresses, as Brown and Booker (1985) developed a procedure to calculate equivalent nodal forces for uncoupled excavation problems.

Nogueira (1998) presented, for coupled analysis of excavation, the following external nodal forces:

$$\mathbf{F}_i = \sum_{e=1}^{\text{numel}_i} \left[\int_{V_e} \mathbf{B}_u^T (\boldsymbol{\sigma}'_{i-1} + \mathbf{N}_p \hat{\mathbf{p}}_{i-1}^e) dV + \int_{V_e} \mathbf{N}_u^T \mathbf{b}^e dV - \int_{S_e} \mathbf{N}_u^T \mathbf{t}^e dS \right] \quad (28)$$

in which $\boldsymbol{\sigma}'_{i-1}$ and $\hat{\mathbf{p}}_{i-1}$ =effective stress and the nodal pore-water pressure vectors on the remaining elements of the previous excavation stage.

The extension of this procedure to submersed excavation under a constant water level is (Nogueira 1998)

$$\mathbf{F}_i = \sum_{e=1}^{\text{numel}_i} \left[\int_{V_e} \mathbf{B}_u^T (\boldsymbol{\sigma}'_{i-1} + \mathbf{N}_p \hat{\mathbf{p}}_{i-1}^e) dV + \int_{V_e} \mathbf{N}_u^T \mathbf{b}^e dV - \int_{S_e} \mathbf{N}_u^T \mathbf{t}^e dS \right] - \mathbf{F}_{wi} \quad (29)$$

in which \mathbf{F}_{wi} =vector of nodal forces equivalent to the boundary water pressure, which can be determined as follows:

$$\mathbf{F}_{wi} = \sum_{e=1}^{\text{numel}_i} \left[\int_{V_e} \mathbf{B}_u^T \mathbf{m} \mathbf{N}_p \hat{\mathbf{p}}_{hid}^e dV + \int_{V_e} \mathbf{N}_u^T \mathbf{b}_w^e dV \right] \quad (30)$$

in which $\hat{\mathbf{p}}_{hid}$ =hydrostatic water pressure vector; $\mathbf{b}_w^T = [0 \ -\gamma_w]$ =body force vector; and γ_w =water's specific weight.

Validation and Use of Coupled Excavation Procedures

One-Dimensional Excavation

The numerical solution accuracy is evaluated by comparing the numerical results of a quick single stage of excavation that removes the top half of a soil column in 500 s, i.e., excavation rate equal to 10^{-2} m/s, against known analytical solutions (Terzaghi 1925). The soil is saturated, linear elastic and under geostatical initial conditions. Fig. 2 shows the finite-element mesh and the boundary conditions in terms of the displacement and pore-water pressure. The Q4Q8 finite element was used, which considers a linear interpolation of pore-water nodal pressures and quadratic

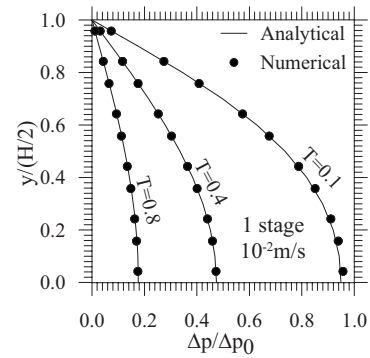


Fig. 3. One-dimensional excavation: excess of pore-water pressure

interpolation of nodal displacements (Nogueira 1998). For the soil, the following properties were adopted: $E=2$ MPa; $\nu=0.3$; $k=10^{-5}$ m/s; and $\gamma_{\text{sat}}=20$ kN/m³.

Figs. 3 and 4 show, respectively, that the numerical results match very well the analytical solution regarding excess of pore-water pressure and superficial displacement of the remaining soil column. In Figs. 3 and 4, the nondimensional time T is defined as: $T=t\{[E(1-\nu)k]/[(1+\nu)(1-2\nu)\gamma_w(H/2)^2]\}$, where γ_w =water specific weight and t =real time. The initial excess of pore-water pressure on the remaining soil column Δp_0 equals 100 kPa (Fig. 3).

A parametric study, considering a single stage of excavation, was conducted in order to assess the influence the hydraulic conductivity and the excavation rate in the pore-water pressure at the remaining column bottom. Fig. 5 shows that an excavation rate 1,000 times higher than the hydraulic conductivity leads to an undrained response. On the other hand, an excavation rate of the same magnitude order as the hydraulic conductivity leads to a drained response.

Fig. 6 shows the total and effective stress paths of a point right above the bottom of the remaining soil column at the end of each five-stage excavation conducted under different rate: slow rate ($\nu=10^{-5}$ m/s) and fast rate ($\nu=10^{-2}$ m/s), both for a hydraulic conductivity of 10^{-5} m/s.

Fig. 6(a) shows that for the slow excavation rate, the effective and the total stress paths are similar indicating a drained response. The effective stress path reproduces the K_0 -line path. Fig. 6(b) shows that for the fast excavation rate, no variation is observed in the normal effective stress p' . The normal effective stress p' starts to vary when the excess of pore-water pressure starts to dissipate due to drainage. After drainage, the effective and total stress states reproduced by the slow and fast excavation are similar.

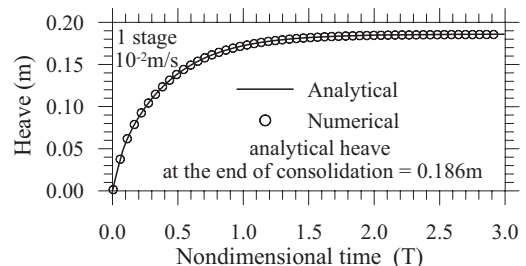


Fig. 4. One-dimensional excavation: superficial displacements of the remaining soil column

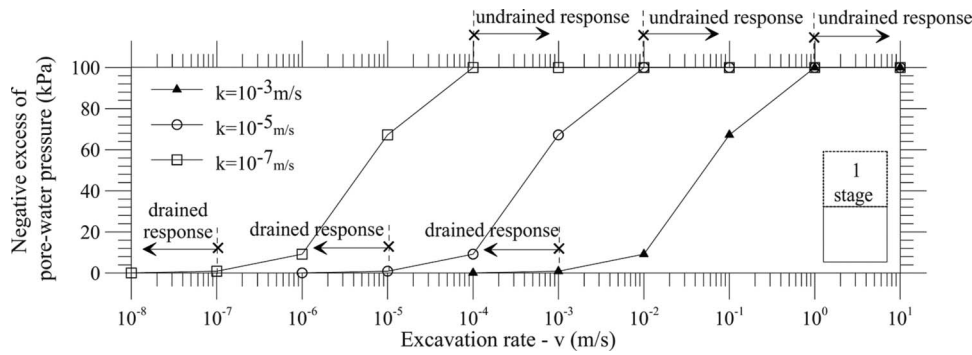


Fig. 5. Excess of pore-water pressure versus excavation rate and hydraulic conductivity

These results indicate that the effective stresses at the bottom of this excavation have not been affected by the time the excavation was completed. This sustains the thesis that the long-term condition is the most critical one for the excavation problems.

Coupled Analysis of Open-Cut Excavations

The coupled finite-element simulation of an open-cut excavation was conducted in order to evaluate the sensitivity of the results to the selected constitutive model. Although the specific excavation evaluated in this study is hypothetical, the geometry and material properties are based on actual projects. Fig. 7 presents the problem's geometry that involves a symmetric open-cut excavation that is 4 m high and 8 m wide. The problem was simulated with a finite-element mesh of 210 Q4Q8 elements and 689 nodal points. The soil material is homogeneous and isotropic with a hydraulic conductivity of 10^{-7} m/s and a saturated self-weight of

18 kN/m^3 . The wall material is homogeneous, isotropic, and linear elastic with the following properties: $E_{\text{wall}}=10 \text{ GPa}$; $\nu_{\text{wall}}=0.3$.

The analyses consider a single excavation stage having three different rates according to one-dimensional excavation: an extremely slow rate, 4 m in 5,000 days, corresponding to 10% of the soil's hydraulic conductivity; an intermediate rate, 4 m in 5 days, or 100 times greater than the soil's hydraulic conductivity; and an extremely fast one, 4 m in 0.005 days, or 10,000 times greater than the soil's hydraulic conductivity. These excavation rates represent, respectively, drained, partially drained, and essentially undrained excavation response.

To represent the soil behavior, the analyses used three constitutive models: linear elastic, nonlinear elastic hyperbolic (Duncan 1980), and nonlinear elastoplastic (Lade 1977). Using the experimental results obtained by Azevedo (1983) the following parameters were achieved for the linear elastic model— $E=20 \text{ MPa}$ and $\nu=0.30$; for the hyperbolic model— $K=342$, $n=0.43$, $K_b=150$, $m=0.45$, $\phi'=31^\circ$, $c'=2.8 \text{ kPa}$, and $R_f=0.91$; and for Lade's model— $K_{ur}=370$, $n=0.51$, $\nu=0.30$, $m=0.076$, $\eta_1=19.4$, $C=0.00095$, $p=0.63$, $w_1=0.2$, $w_2=2.01$, $q_1=4.75$, $q_2=0.79$, $s_1=0.37$, $s_2=0.0$, $t_1=3.49$, and $t_2=-4.12$.

The hyperbolic model was used in this study because it has become the most popular constitutive model in Brazil through the years because of its simplicity, even through presenting some known limitations. The Lade's model was adopted because it proved to be adequate in previous excavation simulation (Azevedo 1983, Zornberg 1989; Nogueira 1998) and was successfully

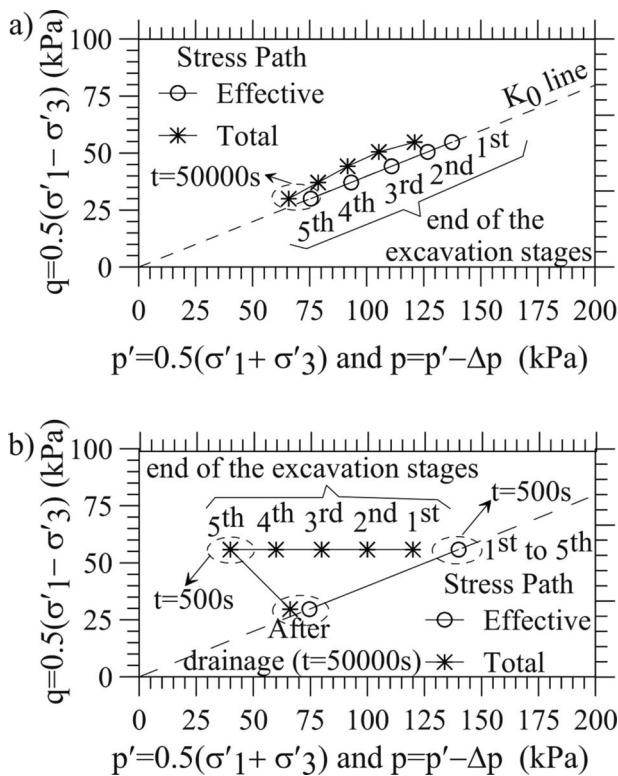


Fig. 6. Stress path for one-dimensional excavation: (a) slow rate; (b) fast rate

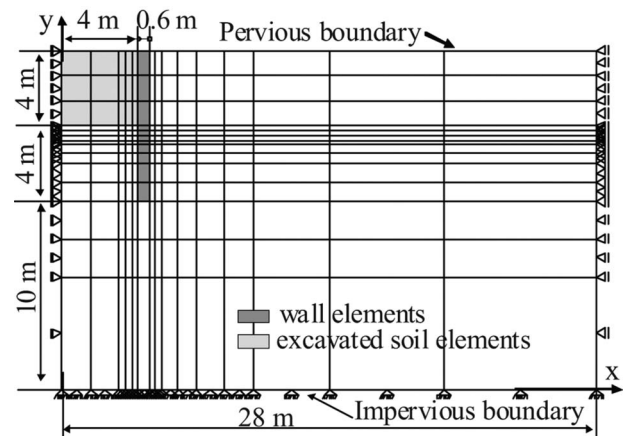


Fig. 7. Open-cut excavations analysis: finite-element mesh

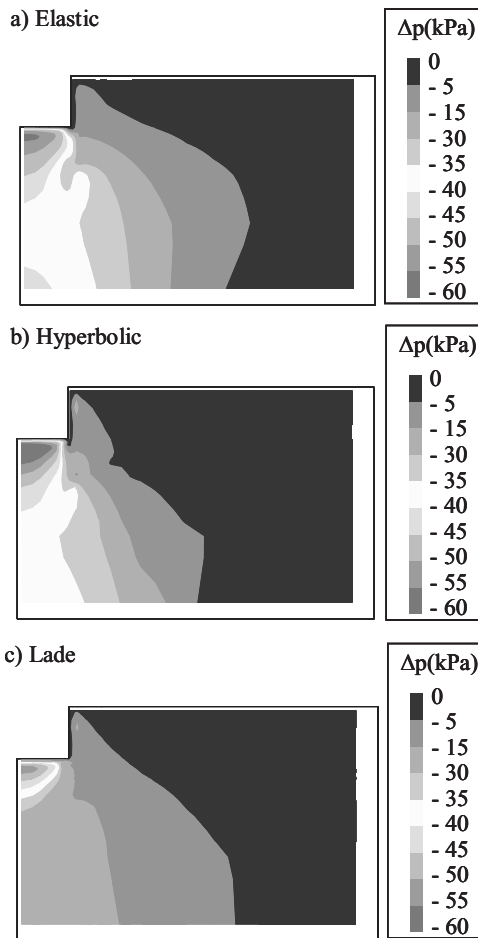


Fig. 8. Excess of pore-water pressure for fast-rate excavation: (a) Elastic; (b) hyperbolic; and (c) Lade

used on a back-analysis of a shallow tunnel through residual soils in Brazil (Azevedo et al. 2002), as it adequately reproduces soil behavior under different stress paths.

The simulations were conducted using automatic load/time increments characterized by an initial factor of time and load increment of 1% (i.e., $\Delta\lambda_t^0 = \Delta\lambda_c^0 = 0.01$) and a tolerance of 0.01% for the desired iterations number I_d of 4.

Fig. 8 shows the isocurves of the pore-water pressure excess at the end of the fast-rate excavation for the constitutive models adopted. The constitutive model affected the magnitude and distribution of the excess of the pore-water pressure, mainly at the bottom of the excavation where the elastoplastic constitutive model provided the highest magnitude. However, the constitutive models slightly influenced the dissipation rate of the excess of the pore-water pressure, as can be noted in Fig. 9.

Fig. 10 shows the short- and long-term surface vertical movements (positive displacement is heave) for the single-stage, fast-rate excavation. The results indicate trends in surface vertical displacement obtained using the linear and nonlinear elastic models are similar. However, the results obtained with the elastoplastic model are different, as downward movements occur at locations adjacent to the wall, in accordance with a possible failure mechanism.

Fig. 11 shows the short- and long-term horizontal displacements profiles at the wall external face for the single-stage, fast-rate excavation. The solution provided by the linear elastic model predicts wall movements that are opposite in direction to those

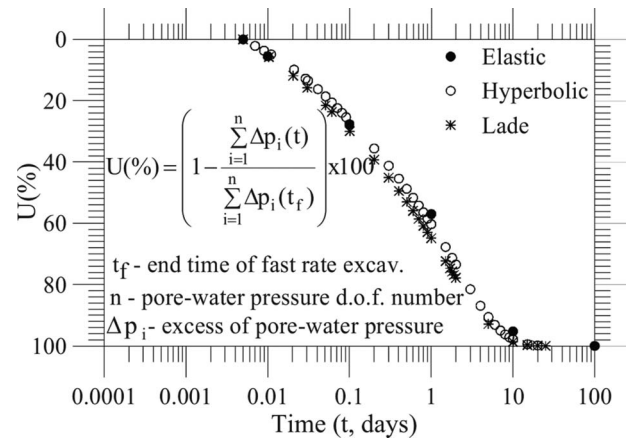


Fig. 9. Average consolidation percentage after fast-rate excavation

obtained with more sophisticated models. In the short-term prediction, the nonlinear elastic and elastoplastic solutions present similar horizontal displacement, Fig. 11(a), but the difference between these two constitutive model solutions becomes greater, Fig. 11(b) at long term.

Fig. 12 presents long-term stress level isocurves for the single-stage, fast-rate excavation conducted using the hyperbolic and Lade's model, respectively. The stress level ratio, for the hyperbolic model, is given by

$$SLR = (0.5(\sigma'_1 - \sigma'_3)) / ((\sigma'_3 \sin \phi + c \cos \phi) / (1 - \sin \phi)) \quad (31a)$$

in which σ'_1 and σ'_3 =principal effective stresses; c =cohesion; and ϕ =friction angle; for the Lade's model, the stress level is given by

$$SLR = ((I_1^3 / I_3 - 27) / (I_1 / p_a)^m) / (\eta_1) \quad (31b)$$

in which I_1 and I_3 =stress invariants and m and η_1 =Lade's model failure parameters.

The elastoplastic solution [Fig. 12(b)] captures more precisely the expected shape of a potential failure surface than the nonlinear elastic model, confirming the downward movement previously mentioned (Fig. 10).

Overall, the analyses conducted for the case of a two-dimensional excavation indicate that the selection of the constitutive model can have significant implications on the predicted movements, particularly for long-term conditions. Also, although the use of a coupled analysis leads to essentially the same long-term deformations as those obtained using drained analyses, coupled simulations allow characterization at the end of construction, which may have significant design implications, mainly related to the support structure definition.

Conclusions

The analyses of two hypothetical excavations illustrate the influence of soil hydraulic properties, rate of excavation construction, and soil constitutive modeling on the performance of excavations by using a finite-element formulation that couples flow and deformation.

The modified Newton-Raphson method used to solve the nonlinear problem, together with automatic sizing of load and time increments, produced good answers in terms of convergence. Fur-

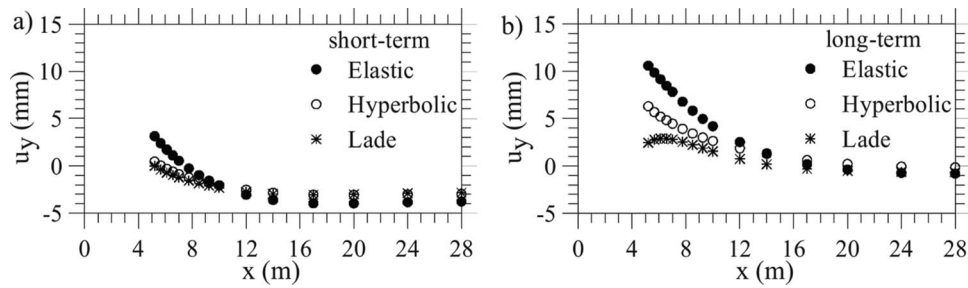


Fig. 10. Vertical displacement at surface (u_y): (a) short term; (b) long term

ther, an explicit stress integration algorithm having variably sized subincrements that are proportional to the strain increment performed well when used for the constitutive model's integrations.

Although the constitutive model affected the magnitude and distribution of the excess of the pore-water pressure due to the excavation process, the constitutive models only slightly influenced the dissipation rate of the excess pore-water pressure.

Results obtained with the elastoplastic model are the only ones that predict downward surface movements in points adjacent to the wall. In accordance with this observation, the elastoplastic solution more precisely captures the shape of a potential failure

surface. The horizontal displacements of the retaining wall obtained by the linear elastic model prediction movements were opposite to those obtained with other models

Based on the results of these investigations, excavation rates that were one order of magnitude smaller than the hydraulic conductivity of the soil led to results representative of drained processes. Because of the slow rate needed for drained conditions, partially drained conditions normally prevail during excavations, highlighting the importance of coupled analyses.

Acknowledgments

The writers are grateful for the financial support received by the first writer from CAPES (Coordinating Agency for Advanced Training of High-Level Personnel—Brazil). They also acknowledge Professor John Whites and Harriet Reis for the editorial review of this text.

References

- Azevedo, R. F. (1983). "Centrifugal and analytical modeling of excavation in sand." Ph.D. thesis, Univ. of Colorado at Boulder, Boulder, Colo.
- Azevedo, R. F., and Consoli, N. C. (1988). "Comparisons between field and analytical behavior of an experimental excavation." *Proc., 2nd Int. Conf. on Case Histories in Geotechnical Engineering*, 1465–1469.
- Azevedo, R. F., Parreira, A. B., and Zornberg, J. G. (2001). "Numerical analysis of a tunnel in residual soil." *J. Geotech. Geoenviron. Eng.*, 128(3), 227–236.
- Biot, M. A. (1941). "General theory of three-dimensional consolidation." *J. Appl. Phys.*, 12, 155–164.
- Booker, J. R., and Small, J. C. (1975). "An investigation of the stability of Biot's equations of consolidation." *Int. J. Solids Struct.*, 11, 907–917.
- Borja, R. I. (1986). "Finite element formulation for transient pore pressure dissipation: A variational approach." *Int. J. Solids Struct.*, 22, 1201–1211.
- Borja, R. I. (1989). "Linearization of elastoplastic consolidation equations." *Eng. Comput.*, 6, 163–168.
- Borja, R. I. (1991). "One-step and linear multistep methods for nonlinear consolidation." *Comput. Methods Appl. Mech. Eng.*, 85, 239–272.
- Borja, R. I., Lee, S. R., and Seed, R. B. (1989). "Numerical simulation of excavation in elastoplastic soils" *Int. J. Numer. Analyt. Meth. Geomech.*, 13, 231–249.
- Brown, P. T., and Booker, J. R. (1985). "Finite element analysis of excavation." *Comput. Geotech.*, 1, 207–220.
- Carter, J. P., Booker, J. R., and Small, J. C. (1979). "The analysis of finite elastoplastic consolidation." *Int. J. Numer. Analyt. Meth. Geomech.*, 3, 107–129.

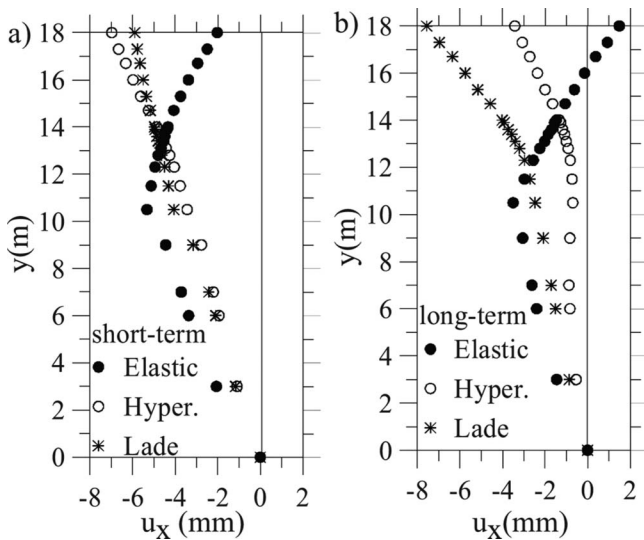


Fig. 11. Horizontal displacements (u_x): (a) short term; (b) long term

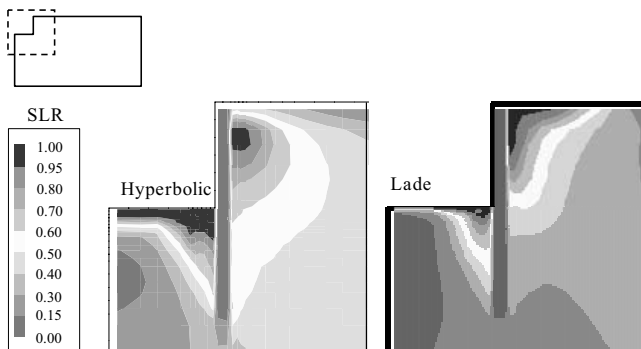


Fig. 12. Stress level ratio for hyperbolic model: (a) short term; (b) long term

- Chandrasekaran, V. S., and King, G. J. (1974). "Simulation of excavations using finite elements." *J. Geotech. Engrg. Div.*, 100(9), 1086–1089.
- Christian, J. T., and Bohemer, J. W. (1970). "Plane strain consolidation by finite elements." *J. Soil Mech. and Found. Div.*, 96(4), 1435–1457.
- Christian, J. T., and Wong, I. H. (1973). "Errors in simulating excavation in elastic media by finite elements." *Soils Found.*, 13(1), 1–10.
- Crisfield, M. (1981). "A fast incremental/iterative solution procedure that handles 'snap-through.'" *Comput. Struct.*, A13, 55–62.
- Duncan, M. J. (1980). "Hyperbolic stress-strain relationships." *Proc., Workshop on Limit Equilibrium, Plasticity and Generalized Stress-Strain in Geotechnical Engineering*, 443–460.
- Ghaboussi, J., and Pecknold, D. A. (1984). "Incremental finite element analysis of geometrically altered structures." *Int. J. Numer. Methods Eng.*, 20, 2051–2064.
- Ghaboussi, J., and Wilson, E. L. (1973). "Flow of compressible fluid in porous elastic media." *Int. J. Numer. Methods Eng.*, 5(3), 419–442.
- Griffiths, D. V., and Li, C. O. (1993). "Analysis of delayed failure in sloping excavations." *J. Geotech. Engrg.*, 119(9), 1360–1378.
- Holt, D. A., and Griffiths, D. V. (1992). "Transient analysis of excavations in soil." *Comput. Geotech.*, 13, 159–174.
- Hwang, C. T., Morgenstern, N. R., and Murray, D. T. (1971). "On solutions of plane strain consolidation problems by finite element methods." *Can. Geotech. J.*, 8(1), 109–118.
- Hwang, C. T., Morgenstern, N. R., and Murray, D. T. (1972). "Application of the finite element method to consolidation problems." *Proc., Symp. Application of the Finite Element Methods in Geotechnical Engineering*, 739–765.
- Lade, P. V. (1977). "Elastoplastic stress-strain theory for cohesionless soils with curved yield surfaces." *Int. J. Solids Struct.*, 3, 1019–1035.
- Mana, A. I. (1978). "Finite element analysis of deep excavation behavior in soft clay." Ph.D. thesis, Stanford Univ., Stanford, Calif.
- Marques, J. M. M. C. (1984). "Stress computation in elastoplasticity." *Eng. Comput.*, 1(4), 2–51.
- Nayak, G. C. and Zienkiewicz, O. C. (1972). "Elastoplastic stress analysis: A generalization for various constitutive laws including strain softening." *Int. J. Numer. Methods Eng.*, 5, 113–135.
- Nogueira, C. L. (1998). "Análise não linear de escavações e aterros." DSc thesis, Pontifícia Universidade Católica do Rio de Janeiro, Rio de Janeiro, Brazil (in Portuguese).
- Ortiz, M., and Popov, E. P. (1985). "Accuracy and stability of integration algorithms for elastoplastic constitutive relations." *Int. J. Numer. Methods Eng.*, 21, 1561–1576.
- Osaimi, A. E. (1977). "Finite element analysis of time dependent deformations and pore pressure in excavation and embankments." Ph.D. thesis, Stanford Univ., Stanford, Calif.
- Potts, D. M., and Ganendra, D. (1994). "An evaluation of substepping and implicit stress point algorithms." *Comput. Methods Appl. Mech. Eng.*, 119, 341–354.
- Richter, T. (1979). "Nonlinear consolidation models for finite element computations." *Proc., 3rd Int. Conf. on Numerical Methods in Geomechanics*, 181–191.
- Sandhu, R. S., Liu, H., and Singh, K. J. (1977). "Numerical performance of some finite element schemes for analysis of seepage in porous elastic media." *Int. J. Numer. Analyt. Meth. Geomech.*, 1, 177–194.
- Siriwardane, H. J., and Desai, C. S. (1981). "Two numerical schemes for nonlinear consolidation." *Int. J. Numer. Methods Eng.*, 17, 405–426.
- Sloan, S. W. (1987). "Substepping schemes for the numerical integration of elastoplastic stress-strain relations." *Int. J. Numer. Methods Eng.*, 24, 893–911.
- Sloan, S. W., Abbo, A. J., and Sheng, D. (2001). "Refined explicit integration of elastoplastic models with automatic error control." *Eng. Comput.*, 18(1), 121–154.
- Terzaghi, K. (1925). *Erdbaumechanik auf bodenphysikalischer Grundlage*, F. Devitke, ed., Viena.
- Whittle, J. A., Hashash, Y. M. A., and Whitman, R. V. (1993). "Analysis of deep excavation in Boston." *J. Geotech. Engrg.*, 119(1), 69–90.
- Yokoo, Y., Yamagata, K., and Nagaoka, H. (1971). "Finite element method applied to Biot's consolidation theory." *Soils Found.*, 11(1), 25–35.
- Yong, K. Y., Lee, F. H., Parnpoy, U., and Lee, S. L. (1989). "Elastoplastic consolidation analysis for strutted excavation in clay." *Comput. Geotech.*, 8, 311–328.
- Zornberg, J. G. (1989). "Análise por elementos finitos do comportamento de escavações utilizando um modelo elasto-plástico." MSc thesis, Pontifícia Universidade Católica do Rio de Janeiro, Rio de Janeiro, Brazil (in Portuguese).